STATIC BENDING ANALYSIS OF BIO-INSPIRED COMPOSITE SHELL INTEGRATED WITH PIEZOELECTRIC SURFACE LAYER

Tran Thi Thu Thuy[1,*], Nguyen Tu Anh[1], Dao Nhu Mai[2], Thanh Trung Nguyen[3]

DOI: https://doi.org/10.57001/huih5804.2026.007

ABSTRACT

This paper presents an isogeometric method based on the modified first-order shear deformation theory (m-FSDT) for static bending analyses of a bio-inspired helicoid laminated composite (B-iHLC) shallow shell integrated with piezoelectric surface layers (hereafter referred to as B-iHLC-Piezo shell), resting on a Pasternak foundation and accounting for initial geometrical imperfections. The shell's core layer is constructed using helicoidal schemes inspired by biological composite structures, which enable high-impact energy absorption with remarkable efficiency and exceptional damage resistance. The surface layers consist of isotropic piezoelectric smart materials capable of actively controlling structural vibrations. The mechanical displacement field is approximated via the m-FSDT framework using Non-Uniform Rational B-Spline (NURBS) basis functions. The reliability and effectiveness of the proposed method are validated through numerical comparisons with existing literature. The findings from this study serve as valuable references for the design and vibration control of advanced structures in military, aerospace, marine, and related engineering fields.

Keywords: *Modified first-order shear hypothesis; IGA; bio-inspired helicoid laminated composite, piezoelectric layer, initial geometrical imperfection.*

[1]School of Mechanical and Automotive Engineering, Hanoi University of Industry, Vietnam

[2]Institute of Mechanics, Vietnam Academy of Science and Technology, Vietnam

[3]Nissan Automotive Technology Vietnam Company, Hanoi, Vietnam

Received: 15/10/2025

Revised: 16/12/2025

Accepted: 28/01/2026

1. INTRODUCTION

Today, numerous studies provide evidence that humans can utilize the unique structures of nature for creation and production. Several studies [1] have investigated sandwich-like structures using honeycomb cores, inspired by natural honeycomb structures. Furthermore, the layer arrangement seen in many natural landforms, such as plants, insects, and mammals, results in enhanced stiffness. By using these arrangements in multilayer structures, significant stiffness can be achieved without compromising flexibility [2]. Currently, research is underway on the development and production of hierarchical structures inspired by natural materials including spider webs, seashells, bones, and flora. The goal is to develop new materials with qualities and functions similar to those found in nature. Researchers want to recreate the hierarchical organization seen in biomaterials to develop materials with superior strength, resilience, and stability, while remaining lightweight and highly durable [3]. Inspired by the spiral layer arrangement in these systems, researchers [4] studied how external objects affect multilayer composite structures. To control the vibrational ability of the structure, it is common to fabricate structures attached to piezoelectric layers, studies such as [5, 6]. Liu et al. [7] analyzed the static and dynamic properties of composite plates incorporating piezoelectric layers using radial point interpolation and first-order shear strain theory. Quang et al. [8] used isogeometric methods to control the vibration of FG-CNT reinforced composite plates with piezoelectric layers based on higher-order shear strain theory. In the aforementioned studies, there is still no significant research on shell structures made of natural composite materials incorporating piezoelectric layers, moreover, the use of higher-order shear strain theories would cause many computational complexities.

In this study, the authors found that classical and first-order shear strain theories were insufficient to accurately predict shear stresses at the upper and lower surfaces of the shell in computational studies. Only more advanced theories, using the g(z) coefficient to quantify the effect of thickness on shear strain, could achieve this. However,

the use of higher-order shear strain theories increases complexity and computational time, requiring more knowledge and resources. To the authors' knowledge, this is the first case where the IGA method combined with a modified first-order shear theory was used to analyze the static bending characteristics of a B-iHLC-Piezo shell placed on a Pasternak foundation, taking into account the initial geometric defects. The biocomposite structures using B-iHLC and the design have the ability to absorb strong impact energy and withstand significant trauma. The core layer of the shell is created by helicoidal schemes and designs in biocomposite structures, allowing them to absorb high impact energy with remarkable efficiency and providing exceptional damage resistance, while the surface layers are made of isotropic piezoelectric smart materials capable of controlling structural vibrations. This study is able to accurately calculate shear stress at both the top and bottom surfaces of the B-iHLC-Piezo double curved shallow shell, thus constituting one of its main advantages. The calculation algorithm presented in the paper is applicable to all shell shapes and is particularly suitable for the B-iHLC-Piezo double curved shallow shell.

2. THEORETICAL BACKGROUND

2.1. Geometric model and shell material

Consider a B-iHLC-Piezo shell structure with two curvatures having a rectangular projection with geometric parameters as shown in Figure 1. The B-iHLC-Piezo cladding consists of three layers of material: the core is B-iHLC material, and the two surface layers are isotropic piezoelectric materials. Attach the structural shell to the Oxyz coordinate system, from which the geometric dimensions can be determined, including length a, width b, and thickness $h = h_c + h_a + h_s$. The B-iHLC-Piezo casing has two distinct radii of curvature, R_x and R_y. The B-iHLC-Piezo shell rests on a Pasternak elastomer, and this medium has two distinct stiffness parameters, namely the spring coefficient k_w and the shear coefficient k_s.

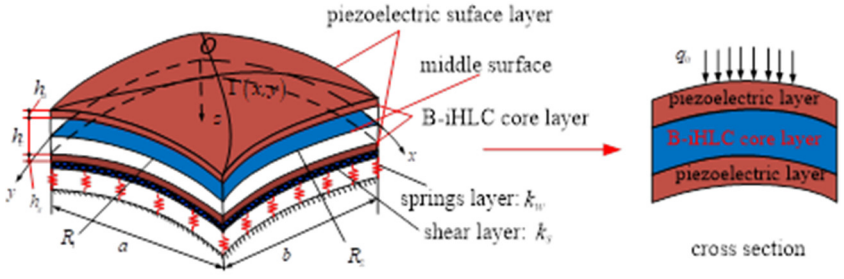

a) The model of B-iHLC-Piezo shell lying on Pasternak medium

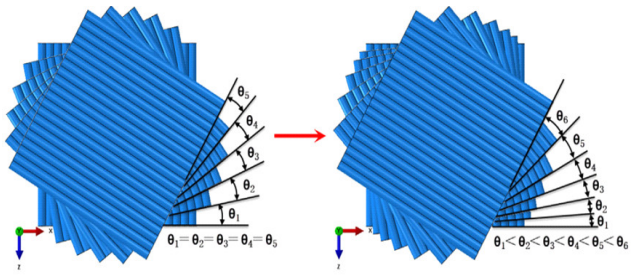

b) Model of B-iHLC core layer

Figure 1. Modeling of a B-iHLC-Piezo shell with initial geometrical imperfection

The laws governing the change in the stacking angle of helicoidal cores are described by the mathematical formulas below [4]:

- Helicoidal-Recursive (HR):

$$\left\{\theta_1 / \theta_2 / \ldots / \theta_n = \theta_{n-1} + \beta(n-1)\right\}, n = 1,2,\ldots,k \quad (1)$$

in which: k and β are the stacking angle and the stacking angle control coefficient, respectively $(\beta \in Z)$.

- Helicoidal-expanding (HE)

$$\left\{\theta_1 / \theta_2 / \ldots / \theta_n = \gamma^n\right\} \quad (2)$$

- Helicoidal-semicircular (HS).

$$\left\{\theta_1 / \theta_2 / \ldots / \theta_n = \sqrt{\varphi^2 - \left(\chi(n-1) - \varphi\right)^2}\right\} \quad (3)$$

where: χ, φ are the control coefficients of the stacking angle law.

2.2. Constituent relationships

Based on Mindlin's first-order shear deformation theory [9], the displacement at any point of the two-curved shell is described as follows:

$$\begin{cases} u(x,y,z) = (1 + z/R_x)u_0(x,y) + z\varphi_x(x,y); \\ v(x,y,z) = (1 + z/R_y)v_0(x,y) + z\varphi_y(x,y); \\ w(x,y,z) = w_0(x,y) + \Gamma(x,y) \end{cases} \quad (4)$$

here u_0, v_0, w_0 represents vertical displacement in three directions x, y and z; φ_x, φ_y are the angular displacements of the point of rotation around the y-axis and the x-axis, respectively. $\Gamma(x, y)$ is called the original geometric defect function and is described by the arithmetic functions in [10].

Based on the displacement field described above, the non-zero linear strain field of the plate is described as follows:

$$\boldsymbol{\varepsilon}_b = \boldsymbol{\varepsilon}_1 + z\boldsymbol{\varepsilon}_2, \boldsymbol{\varepsilon}_s = \boldsymbol{\gamma}_0, \text{ with } \boldsymbol{\gamma}_0 = \begin{Bmatrix} \frac{\partial w_0}{\partial x} + \varphi_x \\ \frac{\partial w_0}{\partial y} + \varphi_y \end{Bmatrix},$$

$$\boldsymbol{\varepsilon}_1 = \begin{Bmatrix} \frac{\partial u_0}{\partial x} + \frac{w_0}{R_x} + \frac{\partial w_0}{\partial x}\frac{\partial \Gamma(x,y)}{\partial x} \\ \frac{\partial v_0}{\partial y} + \frac{w_0}{R_y} + \frac{\partial w_0}{\partial x}\frac{\partial \Gamma(x,y)}{\partial x} \\ \frac{\partial u_0}{\partial y} + \frac{\partial v_0}{\partial x} + \frac{\partial w_0}{\partial x}\frac{\partial \Gamma(x,y)}{\partial y} + \frac{\partial w_0}{\partial y}\frac{\partial \Gamma(x,y)}{\partial x} \end{Bmatrix} \quad (5)$$

$$\boldsymbol{\varepsilon}_2 = \begin{Bmatrix} \frac{\partial \varphi_x}{\partial x} + \frac{\partial u_0}{R_x \partial x} \\ \frac{\partial \varphi_y}{\partial y} + \frac{\partial v_0}{R_y \partial y} \\ \frac{\partial \varphi_x}{\partial y} + \frac{\partial \varphi_y}{\partial x} + \frac{\partial u_0}{R_x \partial y} + \frac{\partial v_0}{R_y \partial x} \end{Bmatrix}$$

The relationship between stress and strain components, and the electric field, taking into account the influence of the piezoelectric layer of the B-iHLC-Piezo shell, is written as follows [7]:

$$\boldsymbol{\sigma}^k = \boldsymbol{S}^k\boldsymbol{\varepsilon} - \boldsymbol{e}^{k\mathrm{T}}\boldsymbol{E}; \boldsymbol{D}^k = \boldsymbol{e}^k\boldsymbol{\varepsilon} + \boldsymbol{g}^k\boldsymbol{E} \quad (6)$$

here: $\boldsymbol{\sigma} = \{\sigma_x, \sigma_y, \tau_{xy}, \tau_{yz}, \tau_{zx}\}^T$ is the stress vector; $\boldsymbol{S}$ is the material stiffness matrix of the k-th layer, and it is defined as follows:

$$\boldsymbol{S}^k = \begin{bmatrix} \boldsymbol{Q}_b^k & [0] \\ [0] & \boldsymbol{Q}_s^k \end{bmatrix}; \boldsymbol{Q}_b^k = \begin{bmatrix} Q_{11} & Q_{12} & 0 \\ Q_{12} & Q_{22} & 0 \\ 0 & 0 & Q_{66} \end{bmatrix}^k; \quad (7)$$

$$\boldsymbol{Q}_b^k = \begin{bmatrix} Q_{44} & 0 \\ 0 & Q_{55} \end{bmatrix}^k$$

Q_{ij} are the stiffness coefficients of the composite material [7]. $\boldsymbol{E}$ is the electric field intensity vector, determined through the voltage transformation as follows:

$$\boldsymbol{E}_v = -\nabla\phi = \{0 \quad 0 \quad E^z\}^T \quad (8)$$

and $\boldsymbol{D}$ is the induced charge vector; - $\boldsymbol{e}$ is the piezoelectric coefficient matrix and $\boldsymbol{g}$ is the dielectric constant matrix of the piezoelectric layers. These components are identified as follows:

$$\boldsymbol{e}^k = \begin{bmatrix} 0 & 0 & 0 \\ 0 & 0 & 0 \\ 0 & d_{31} & d_{32} \end{bmatrix}^k \begin{bmatrix} Q_{11} & Q_{12} & 0 \\ Q_{12} & Q_{22} & 0 \\ 0 & 0 & Q_{66} \end{bmatrix}^k,$$

$$\boldsymbol{g}^k = \begin{bmatrix} p_{11} & 0 & 0 \\ 0 & p_{22} & 0 \\ 0 & 0 & p_{33} \end{bmatrix}^k \quad (9)$$

here d_{31} and d_{32} are the piezoelectric coefficients; p_{11}, p_{22} and p_{33} are the dielectric constants.

Next, the elastic strain potential variation of the B-iHLC-Piezo shell is determined as follows [11]:

$$\delta U = \int_{S_e} \left(\delta\boldsymbol{\varepsilon}_b^T \begin{bmatrix} \boldsymbol{A} & \boldsymbol{B} \\ \boldsymbol{B} & \boldsymbol{L} \end{bmatrix} \boldsymbol{\varepsilon}_b + \delta\boldsymbol{\varepsilon}_s^T \boldsymbol{A}_s \boldsymbol{\varepsilon}_s \right) dxdy - \int_{V_e} \delta\boldsymbol{E}^T \boldsymbol{D} dV_e \quad (10)$$

Where S_e, V_e are the surface area and volume of the shell element, respectively. $\boldsymbol{A}$, $\boldsymbol{B}$, $\boldsymbol{L}$, $\boldsymbol{A}_s$ are the material stiffness matrices of the shell, which are defined as follows:

$$\{\boldsymbol{A}, \boldsymbol{B}, \boldsymbol{L}\} = \sum_{k=1}^{n} \int_{z_k}^{z_{k+1}} \boldsymbol{Q}_b^k (1, z, z^2) dz,$$

$$\boldsymbol{A}_s = \sum_{k=1}^{n} \int_{z_k}^{z_{k+1}} \boldsymbol{Q}_s^k G(z) dz \quad (11)$$

$G(z)$ is the shear correction factor; in this study, this factor was chosen as:

$$G(z) = \boldsymbol{\lambda}(1 - z^2/h^2), \boldsymbol{\lambda} = 5/3.89 \quad (12)$$

The strain energy of elastic foundation δU_f is determined by the following formula [12]:

$$\delta U_f = \int_{S_e} \begin{pmatrix} k_w w_0 \delta w_0 + k_s \frac{\partial w_0}{\partial x}\frac{\partial \delta w_0}{\partial x} \\ + k_s \frac{\partial w_0}{\partial y}\frac{\partial \delta w_0}{\partial y} \end{pmatrix} dxdy \quad (13)$$

The total work done by the external force components is determined as follows [13]:

$$\delta V = \int_{\Gamma_S} \boldsymbol{f}_s \delta\boldsymbol{u} d\Gamma_S - \int_{\Gamma_\phi} \boldsymbol{q}_s \delta\boldsymbol{\phi} d\Gamma_\phi + \sum \boldsymbol{F}_p \delta\boldsymbol{u}^T - \sum \boldsymbol{Q}_p \delta\boldsymbol{\phi}^T \quad (14)$$

in which $\boldsymbol{f}_s$ and $\boldsymbol{F}_p$ are the components of the mechanical force acting on the shell surface, respectively. $\boldsymbol{q}_s$ and $\boldsymbol{Q}_p$ are the surface charge and point charge, respectively. Γ_S and Γ_ϕ are the external mechanical load surface and the electrical load surface, respectively.

According to Hamilton's principle [14], the weak form describes the static equilibrium state of the two-curvature shell as follows:

$$\int_{S_e}\begin{pmatrix}\delta\boldsymbol{\varepsilon}_b^T\begin{bmatrix}\boldsymbol{A} & \boldsymbol{B}\\ \boldsymbol{B} & \boldsymbol{L}\end{bmatrix}\boldsymbol{\varepsilon}_b+k_s\dfrac{\partial w_0}{\partial x}\dfrac{\partial\delta w_0}{\partial x}\\ +k_s\dfrac{\partial w_0}{\partial y}\dfrac{\partial\delta w_0}{\partial y}\\ +\delta\boldsymbol{\varepsilon}_s^T\boldsymbol{A}_s\boldsymbol{\varepsilon}_s+k_w w_0\delta w_0\end{pmatrix}dxdy-\int_{V_e}\delta\boldsymbol{E}^T\boldsymbol{D}dV_e$$
$$=\int_{\Gamma_S}\boldsymbol{f}_s\delta\boldsymbol{u}d\Gamma_S-\int_{\Gamma_\phi}\boldsymbol{q}_s\delta\boldsymbol{\phi}d\Gamma_\phi+\sum\boldsymbol{F}_p\delta\boldsymbol{u}^T-\sum\boldsymbol{Q}_p\delta\boldsymbol{\phi}^T \quad (15)$$

3. ISOGEOMETRIC APPROACH

Based on the NURBS function [15], the shell displacement components u_0, v_0, w_0, φ_x, φ_y can be approximated as follows:

$$u_0=\sum_{e=1}^{N_e}\begin{bmatrix}\boldsymbol{R}_e & 0 & 0 & 0 & 0\end{bmatrix}\overline{\boldsymbol{q}}_e=\sum_{e=1}^{N_e}\boldsymbol{X}_e^u\overline{\boldsymbol{q}}_e,$$
$$v_0=\sum_{e=1}^{N_e}\begin{bmatrix}0 & \boldsymbol{R}_e & 0 & 0 & 0\end{bmatrix}\overline{\boldsymbol{q}}_e=\sum_{e=1}^{N_e}\boldsymbol{X}_e^v\overline{\boldsymbol{q}}_e \quad (16a)$$

$$w_0=\sum_{e=1}^{N_e}\begin{bmatrix}0 & 0 & \boldsymbol{R}_e & 0 & 0\end{bmatrix}\overline{\boldsymbol{q}}_e=\sum_{e=1}^{N_e}\boldsymbol{X}_e^w\overline{\boldsymbol{q}}_e,$$
$$\varphi_x=\sum_{e=1}^{N_e}\begin{bmatrix}0 & 0 & 0 & \boldsymbol{R}_e & 0\end{bmatrix}\overline{\boldsymbol{q}}_e=\sum_{e=1}^{N_e}\boldsymbol{X}_e^x\overline{\boldsymbol{q}}_e \quad (16b)$$

$$\varphi_y=\sum_{e=1}^{N_e}\begin{bmatrix}0 & 0 & 0 & 0 & \boldsymbol{R}_e\end{bmatrix}\overline{\boldsymbol{q}}_e=\sum_{e=1}^{N_e}\boldsymbol{X}_e^y\overline{\boldsymbol{q}}_e \quad (16c)$$

here $\boldsymbol{R}_e$ and $\overline{\boldsymbol{q}}_e$ respectively represent the unknown shape function and displacement vector at the control point e and $N_e = (p + 1)(q + 1)$ is the number of control points on each physical element. By substituting Eq. (16) into Eq. (), the paper obtains the system of equations describing the electromechanical equilibrium state of the shell as follows:

$$\begin{bmatrix}\boldsymbol{K}_{uu} & \boldsymbol{K}_{u\varphi}\\ \boldsymbol{K}_{\varphi u} & \boldsymbol{K}_{\varphi\varphi}\end{bmatrix}\begin{Bmatrix}\overline{\boldsymbol{q}}\\ \boldsymbol{\Phi}\end{Bmatrix}=\begin{Bmatrix}\boldsymbol{f}\\ \boldsymbol{Q}\end{Bmatrix} \quad (17)$$

In which:

$$\boldsymbol{K}_{uu}=\boldsymbol{K}_L^e+\boldsymbol{K}_f^e,\boldsymbol{K}_{u\varphi}=\int_{S_e}\boldsymbol{B}_u^T\boldsymbol{e}^T\boldsymbol{B}_\Phi dxdy,\boldsymbol{K}_{\varphi u}=\boldsymbol{K}_{u\varphi}^T,$$
$$\boldsymbol{K}_L^e=\int_{S_e}\boldsymbol{B}_u^T\begin{bmatrix}\boldsymbol{A} & \boldsymbol{B} & \boldsymbol{0}\\ \boldsymbol{B} & \boldsymbol{L} & \boldsymbol{0}\\ \boldsymbol{0} & \boldsymbol{0} & \boldsymbol{A_s}\end{bmatrix}\boldsymbol{B}_u dxdy, \quad (18)$$

$$\boldsymbol{K}_f^e=\int_{S_e}\begin{pmatrix}k_w\boldsymbol{X}_e^{wT}\boldsymbol{X}_e^w+k_s\dfrac{\partial\boldsymbol{X}_e^{wT}}{\partial x}\dfrac{\partial\boldsymbol{X}_e^w}{\partial x}\\ +k_s\dfrac{\partial\boldsymbol{X}_e^{wT}}{\partial y}\dfrac{\partial\boldsymbol{X}_e^w}{\partial y}\end{pmatrix}dxdy,$$
$$\boldsymbol{K}_{\varphi\varphi}=\int_{S_e}\boldsymbol{B}_\Phi^T\boldsymbol{g}^T\boldsymbol{B}_\Phi dxdy, \quad (19)$$

$$\boldsymbol{f}=\int_{S_e}q\boldsymbol{X}_e^{wT}dxdy,\boldsymbol{B}_u^T=\begin{bmatrix}\boldsymbol{B}_b^1 & \boldsymbol{B}_b^2 & \boldsymbol{B}_s^1\end{bmatrix},$$
$$\boldsymbol{B}_\Phi^T=\begin{bmatrix}0 & 0 & 1/h_a & 0 & 0 & 0\\ 0 & 0 & 0 & 0 & 0 & 1/h_s\end{bmatrix} \quad (20)$$

Here, the electro-mechanical strain matrices are defined as follows:

$$\boldsymbol{B}_b^1=\begin{bmatrix}\dfrac{\partial\boldsymbol{X}_e^u}{\partial x}+\dfrac{\boldsymbol{X}_e^w}{R_x}+\dfrac{\partial\boldsymbol{X}_e^w}{\partial x}\dfrac{\partial\Gamma(x,y)}{\partial x}\\ \dfrac{\partial\boldsymbol{X}_e^v}{\partial y}+\dfrac{\boldsymbol{X}_e^w}{R_y}+\dfrac{\partial\boldsymbol{X}_e^w}{\partial x}\dfrac{\partial\Gamma(x,y)}{\partial x}\\ \dfrac{\partial\boldsymbol{X}_e^u}{\partial y}+\dfrac{\partial\boldsymbol{X}_e^v}{\partial x}+\dfrac{\partial\boldsymbol{X}_e^w}{\partial x}\dfrac{\partial\Gamma(x,y)}{\partial y}+\dfrac{\partial\boldsymbol{X}_e^w}{\partial y}\dfrac{\partial\Gamma(x,y)}{\partial x}\end{bmatrix},$$
$$\boldsymbol{B}_b^2=\begin{bmatrix}\dfrac{\partial\boldsymbol{X}_e^x}{\partial x}+\dfrac{\partial\boldsymbol{X}_e^u}{R_x\partial x}\\ \dfrac{\partial\boldsymbol{X}_e^y}{\partial y}+\dfrac{\partial\boldsymbol{X}_e^v}{R_y\partial y}\\ \dfrac{\partial\boldsymbol{X}_e^x}{\partial y}+\dfrac{\partial\boldsymbol{X}_e^y}{\partial x}+\dfrac{\partial\boldsymbol{X}_e^u}{R_x\partial y}+\dfrac{\partial\boldsymbol{X}_e^v}{R_y\partial x}\end{bmatrix}, \quad (21)$$
$$\boldsymbol{B}_s^1=\begin{bmatrix}\dfrac{\partial\boldsymbol{X}_e^w}{\partial x}+\boldsymbol{X}_e^x\\ \dfrac{\partial\boldsymbol{X}_e^w}{\partial y}+\boldsymbol{X}_e^y\end{bmatrix}$$

By solving Eq. (17) we will obtain the displacement, strain and stress components of the corresponding structure.

4. RESULTS AND DISCUSSION

In this section, Matlab 2018a software is used to develop a static bending calculation program based on the IGA formulas established in sections 2 and 3. The input parameters for the core material and piezoelectric layer are given in Table 1. For ease of comparison of the numerical results of this paper with other accurate results published in the literature, dimensionless result formats are used as follows:

$$w_1 = w_0\left(\frac{a}{2},\frac{b}{2}\right)\frac{100E_{22}h^3}{q_0a^4}, K_w = \frac{k_wa^4}{D_{22}},$$

$$K_s = \frac{k_sa^2}{D_{22}}, D_{22} = \frac{E_{22}h^3}{12}$$

Table 1. Mechanical properties of the material layers [8]

Mechanical properties	B-iHLC core		Piezoelectric layer	
	Core 1	Core 2	PZT-4 (P1)	PZTG1195N (P2)
Elastic modul				
E_{11} (GPa)	172.375		81.3	63
E_{22} (GPa)	6.895		81.3	63
E_{33} (GPa)	-		64.5	63
G_{12} (GPa)	3.4475	-	30.6	24.2
G_{13} (GPa)	1.379	-	25.6	24.2
G_{23} (GPa)	3.4475	-	25.6	24.2
v_{12}	0.25	0.3	0.33	0.3
v_{13}	0.25	0.3	0.43	0.3
v_{23}	0.25		0.43	0.3
Piezoelectric constants				
d_{31} (m/V)	-	-	-1.22e-10	2.54e-10
d_{32} (m/V)	-	-	-1.22e-10	2.54e-10
dielectric constant				
p_{11} (F/m)	-	-	13.1e-9	15.3e-9
p_{22} (F/m)	-	-	13.1e-9	15.3e-9
p_{33} (F/m)	-	-	11.5e-9	15.0e-9

Previous studies have shown that, for the rectangular plate structure problem using the isogeometric part method based on the NUBRS function, the calculation results achieve reliable convergence when the number of control points is 11×11 and the degree of the function is p(q) = 4 [16]. Therefore, in this study, the number of control points is 11x11 and the degree of the element is p(q) = 4 used for all investigations in this study.

First, Table 2 describes a comparison of dimensionless deflection values of a spherical shell ($R = R_x = R_y$) made of layered composite material subjected to uniformly distributed load. The composite material parameters are given in Table 1 and the comparison results are published by Reddy [17] with the layering angle in degrees [0 / 90 / 90 / 0]. From the data table, it can be seen that the results proposed in this paper are in complete agreement with the published results.

Table 2. Comparison of dimensionless deflection of layered composite spherical shells subjected to uniformly distributed load

R/a	$10w_1$			
	a/h = 100		a/h = 10	
	Reddy [17]	This paper	Reddy [17]	This paper
1	0.0715	0.0715	4.8366	4.8370
2	0.2844	0.2844	8.0517	8.0515
3	0.6246	0.6246	9.1463	9.1458
4	1.0559	1.0559	9.5999	9.5993

Next, in Figure 2, a comparison of the centerline deflection values of the square composite plate subjected to a uniformly distributed load and different actuator input voltages was found. The input parameters of plate shape and material can be found in the study of Liu et al. [7]. It can be seen that, when there is a change in the voltage value U, the centerline deflection values proposed by the thesis show similarity in shape and strength accuracy compared to the results of Liu et al. [7].

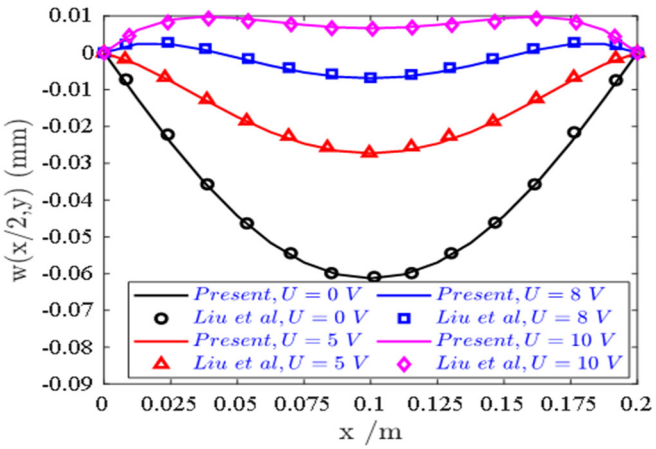

Figure 2. Centerline deviation of the composite plate subjected to different actuator input voltages (SSSS, [p/−45/45]s)

To evaluate the influence of several material factors and electrical boundary conditions on the static bending capacity of the structure, several numerical surveys were performed with the following input parameters: $a = b = 0.2m$, $h_c = 0.1a$, $h_a = h_s = 0.1h_c$, $K_w = 100$, $U = 0V$, $K_s = 10$, $R_x = 5a$, $R_y = 5b$, $g_0/h = 0.1$. The shell is subjected to a uniformly distributed load with intensity $q_0 = 10^4 N/m^2$.

The effect of the actuator voltage applied to the B-iHCL-piezo U casing on the vertical deflection response curve of the B-iHCL-piezo casing is described in Figures 3, 4, and 5. The voltage values applied to the casing are 0V, 20V, 50V, 60V, and 70V when using SSSS boundary conditions; the voltage values are -100V, -50V, 0V, 50V, and 100V when using CFFF boundary conditions; and with CSCS boundary

conditions, the voltage values applied are 0V, 40V, 80V, 120V, and 140V. It is easy to see that the vertical deflection decreases as the input voltage increases, as expected. This is because the input voltage creates an electric force that causes the vertical deflection to be upward, opposite to the direction of the mechanical load due to the piezoelectric effect. This upward contribution becomes common for input voltages of 70V for the SSSS boundary, 100V for the CFFF boundary, and 140V for the CSCS boundary. From this, we also understand that to increase the deflection value of the structure, the direction of the voltage can be changed; in this case, the voltage also causes deflection in the same direction as the mechanical load. Furthermore, we also realize that as the number of core material layers increases, the structure becomes softer and therefore significantly increases the deflection (Figure 4). Along with that, the thinner the core layer, the greater the deflection value (Figure 5), which shows that the stiffness of the shell structure decreases as the core layer thickness decreases.

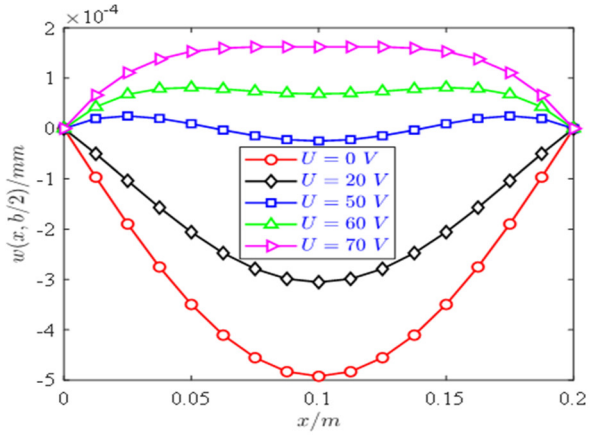

a) $R_x = 5a$, $R_y = 5b$

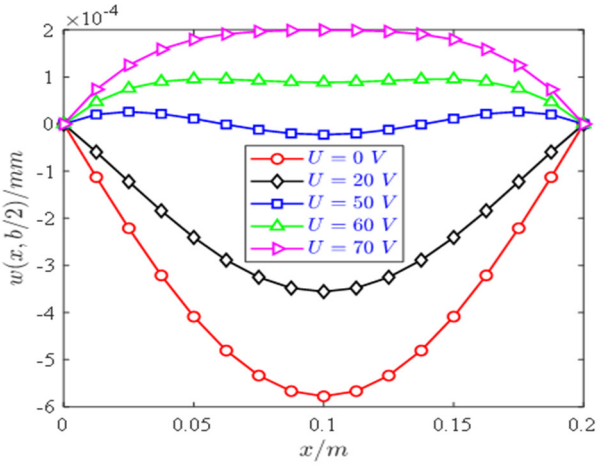

b) $R_x = 5a$, $R_y = -5b$

Figure 3. Vertical deflection curve of rectangular B-iHCL-piezo shell using [P1/HR/P1] material with voltage variation (β = 2, 28 layers, SSSS)

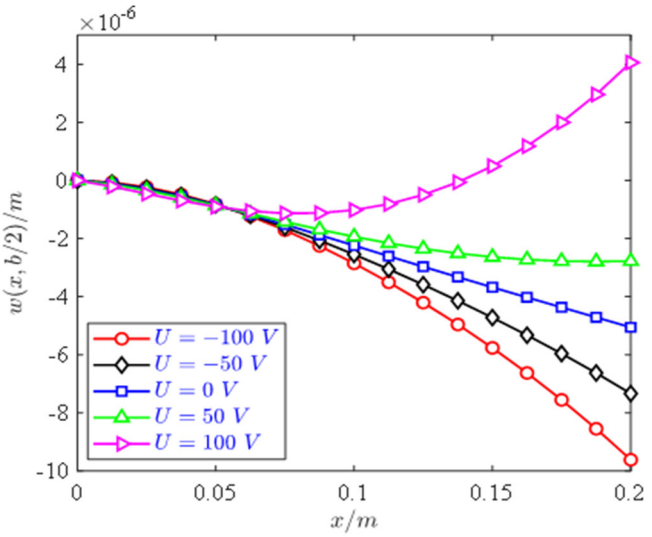

a) 28 layers

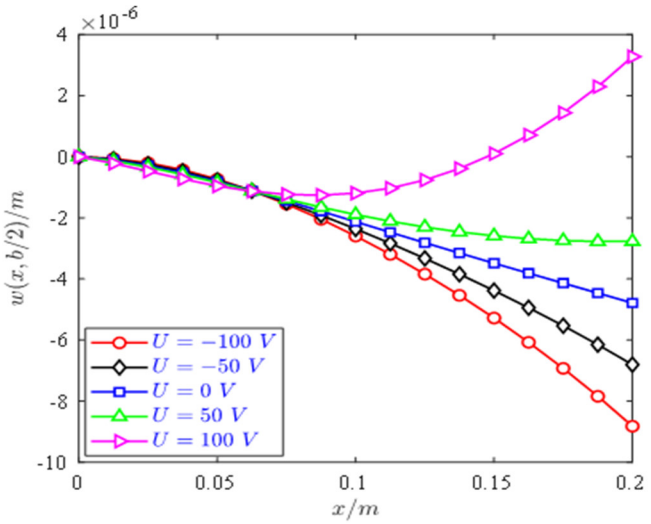

b) 20 layers

Figure 4. Deflection curve w1 of rectangular B-iHCL-piezo spherical shell using [P2/HE/P2] material with varying voltage (β = 2.5, CFFF)

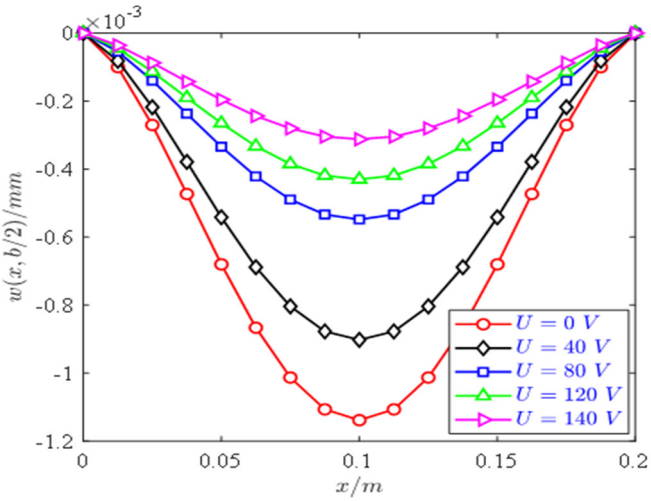

a) $h_c = 0.05a$

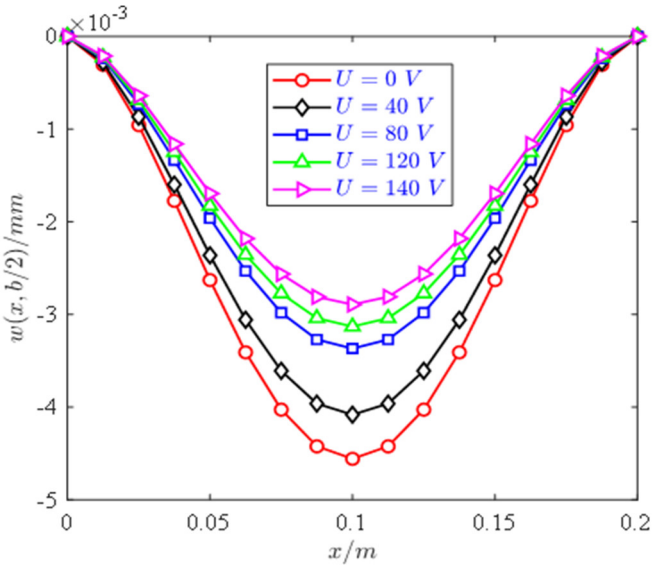

b) $h_c = 0.02a$

Figure 5. Vertical deflection curve of a rectangular B-iHCL-piezo shell using [P1/HS/P1] material with varying applied voltage (φ = 60, χ = 5, 28 layers, SCSC)

Next, the superiority of the improved first-order shear theory is demonstrated in the calculation of normal and tangential stresses of curved shells. The main advantage of this improved theory is that it does not require the use of shear correction factors, and the tangential stress is zero on the top and bottom surfaces of the shell (previously, only higher-order shear strain theory could accurately calculate the tangential stress $\sigma_{xz}(z)$ on the top and bottom surfaces of the structure). The effect of the input voltage U on the shape and values of the normal stresses $\sigma_{xx}(z)$ and tangential stresses $\sigma_{xz}(z)$ along the thickness direction at the midpoint of the plate and shell structure with type C defects is described in Figure 6. In this example, the voltage U is varied with five values: 0V, 20V, 30V, 50V, and 70V, and applied to the B-iHLC-Piezo shell with a rectangular plane and SSSS boundary conditions. It can be seen that, as the voltage U is applied to the structure, the stress values $\sigma_{xx}(z)$ on the top surface of the shell change from positive to negative, and the stress $\sigma_{xx}(z)$ on the bottom surface changes in the opposite direction. This occurs because the voltage U applied to the shell creates a force vector opposite in direction to the force vector created by the initial mechanical force. Here, we also understand that, when the voltage U is reversed, the effect of the electric force will be in the same direction as the mechanical force. Furthermore, for a flat plate-shaped B-iHLC-Piezo shell structure, with symmetrical material and regardless of the influence of geometric defects (see Figure 6a), we see that the stress $\sigma_{xx}(z)$ will have a symmetrical shape with a deviation on z = 0 and $\sigma_{xx}(z) = 0$; in other cases (see Figure 6b) this does not occur $\sigma_{xx}(z) = 0$ and at $z_0 < 0$.

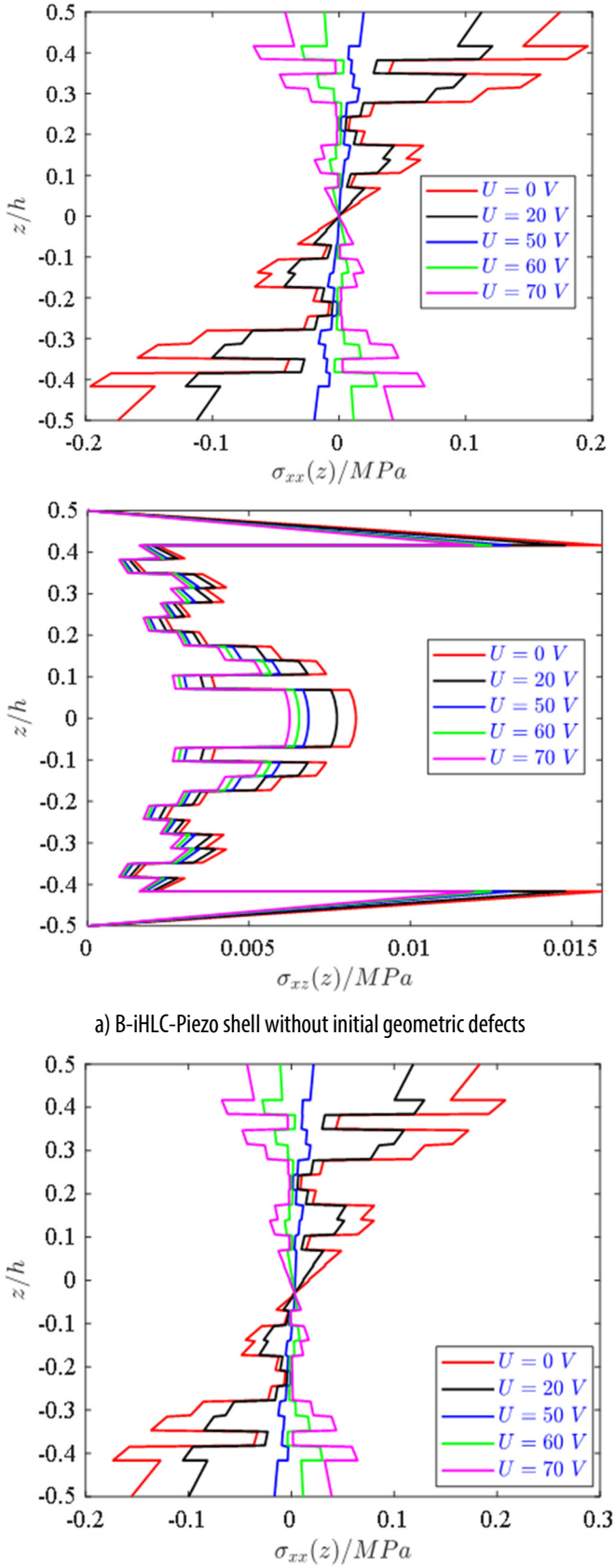

a) B-iHLC-Piezo shell without initial geometric defects

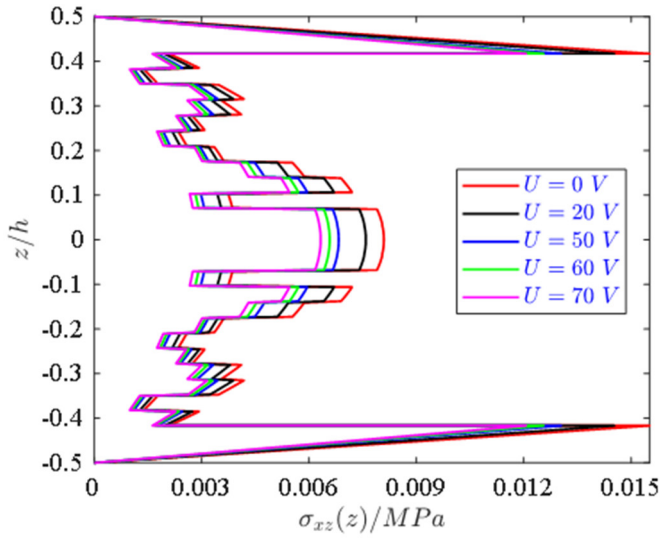

b) B-iHLC-Piezo shell with initial geometric defects

Figure 6. Effect of voltage U on stress of B-iHLC-Piezo shell with geometric defect type C ([P1/HR/P1], β = 2, 24 layers, SSSS)

5. CONCLUSION

Based on the isogeometric method and the improved first-order shear strain theory, the natural static bending and vibration responses of a bio-inspired composite shell integrated with a piezoelectric surface layer, taking into account the initial geometric defects, have been discovered. The improved first-order shear strain theory has several advantages, including eliminating the need for shear correction factors, avoiding shear lock-up, and achieving zero shear stress on both the upper and lower surfaces. The results of this study have clarified the influence of shell geometry parameters, bio-inspired composite materials, piezoelectric materials, mechanical boundary conditions, and electrical boundary conditions on the bending and vibration behavior of a two-curved shell. These results can be applied in vibration control devices, power batteries, and microelectromechanical devices for civilian and military industries.

REFERENCES

[1]. H. A. Pham, H. Q. Tran, M. T. Tran, V. L. Nguyen, Q. T. Huong, "Free vibration analysis and optimization of doubly-curved stiffened sandwich shells with functionally graded skins and auxetic honeycomb core layer," *Thin-Walled Struct.*, 179, 2022. doi: 10.1016/j.tws.2022.109571.

[2]. H. Wan, H. Ohtaki, S. Kotosaka, G. Hu, "A study of negative Poisson's ratios in auxetic honeycombs based on a large deflection model," *Eur. J. Mech. A/Solids*, 23, 1, 95-106, 2004. doi: 10.1016/j.euromechsol.2003.10.006.

[3]. X. Zhu, J. Zhang, W. Zhang, J. Chen, "Vibration frequencies and energies of an auxetic honeycomb sandwich plate," *Mech. Adv. Mater. Struct.*, 26, 23, 1951-1957, 2019. doi: 10.1080/15376494.2018.1455933.

[4]. T. Tran Thi Thu, T. Nguyen Anh, H. Nguyen Thi, H. Nguyen Thi, "Transient response of doubly-curved bio-inspired composite shells resting on viscoelastic foundation subject to blast load using improved first-order shear theory and isogeometric approach," *Def. Technol.*, 38, 171-193, 2024. doi: 10.1016/j.dt.2024.02.003.

[5]. J. Wang, J. Yang, "Higher-order theories of piezoelectric plates and applications," *Appl. Mech. Rev.*, 53, 4, 87-99, 2000. doi: 10.1115/1.3097341.

[6]. H. F. Tiersten, "Linear Piezoelectric Plate Vibrations: Elements of the Linear Theory of Piezoelectricity and the Vibrations Piezoelectric Plates," *Linear Piezoelectric Plate Vibrations, Elements of the Linear Theory of Piezoelectricity and the Vibrations Piezoelectric Plates*, Springer, New York, 2013.

[7]. G. R. Liu, K. Y. Dai, K. M. Lim, "Static and vibration control of composite laminates integrated with piezoelectric sensors and actuators using the radial point interpolation method," *Smart Mater. Struct.*, 13, 6, 1438-1447, 2004. doi: 10.1088/0964-1726/13/6/015.

[8]. K. Nguyen-Quang, T. Vo-Duy, H. Dang-Trung, T. Nguyen-Thoi, "An isogeometric approach for dynamic response of laminated FG-CNT reinforced composite plates integrated with piezoelectric layers," *Comput. Methods Appl. Mech. Eng.*, 332, 25-46, 2018. doi: 10.1016/j.cma.2017.12.010.

[9]. H. M. Ma, X. L. Gao, J. N. Reddy, "A non-classical Mindlin plate model based on a modified couple stress theory," *Acta Mech.*, 220, 1-4, 217-235, 2011. doi: 10.1007/s00707-011-0480-4.

[10]. X. Chen, Y. Lu, Z. Wu, Y. Shao, X. Xue, Y. Wu, "Free vibration of in-plane bi-directional functionally graded materials rectangular plates with geometric imperfections and general elastic restraints," *Aerosp. Sci. Technol.*, 132, 2023. doi: 10.1016/j.ast.2022.108045.

[11]. T. H. Quoc, V. Van Tham, T. M. Tu, "Active vibration control of a piezoelectric functionally graded carbon nanotube-reinforced spherical shell panel," *Acta Mech.*, 232, 3, pp. 1005–1023, 2021. doi: 10.1007/s00707-020-02899-x.

[12]. P. Van Vinh, "On the damped vibration analysis of functionally graded porous beams resting on viscoelastic medium using higher-order shear deformation theory," *J. Vib. Eng. Technol.*, 13, 6, 2025. doi: 10.1007/s42417-025-01954-y.

[13]. T. Liu, C. Li, C. Wang, W. Hu, T. Q. Bui, "Geometrically nonlinear isogeometric analysis of smart piezoelectric FG plates considering thermal effects of piezoelectric stress and dielectric constants," *Compos. Struct.*, 266, 2021. doi: 10.1016/j.compstruct.2021.113795.

[14]. Q. H. Pham, P. C. Nguyen, V. K. Tran, Q. X. Lieu, T. T. Tran, "Modified nonlocal couple stress isogeometric approach for bending and free vibration analysis of functionally graded nanoplates," *Eng. Comput.*, 39, 1, 993-1018, 2023. doi: 10.1007/s00366-022-01726-2.

[15]. T. J. R. Hughes, J. A. Cottrell, Y. Bazilevs, "Isogeometric analysis: CAD, finite elements, NURBS, exact geometry and mesh refinement," *Comput. Methods Appl. Mech. Eng.*, 194, 39-41, 4135-4195, 2005. doi: 10.1016/j.cma.2004.10.008.

[16]. P. H. Tu, T. Van Ke, V. K. Trai, L. Hoai, "An isogeometric analysis approach for dynamic response of doubly-curved magneto electro elastic composite shallow shell subjected to blast loading," *Def. Technol.*, 41, 159-180, 2024. doi: 10.1016/j.dt.2024.06.005.

[17]. J. N. Reddy, "Mechanics of Laminated Composite Plates and Shells," *Mech. Laminated Compos. Plates Shells*, 2003. doi: 10.1201/b12409.